Drying characteristics of biological porous media during convective drying

Wang Huilin[1], Lu Tao[2*], Zhang Quanguo[3]

(1. *College of Energy and Power Engineering, Zhengzhou University of Light Industry, Zhengzhou 450002, China*;
2. *School of Mechanical and Electrical Engineering, Beijing University of Chemical Technology, Beijing 100029, China*;
3. *College of Mechanical and Electrical Engineering, Henan Agricultural University, Zhengzhou 450002, China*)

Abstract: Experiments with potatoes were carried out in order to analyze the variation of the temperature and the mean dry basis moisture content over time, the effect of the drying conditions on the drying rate, and the relationship between deformation and dry basis moisture content. A two-way sequentially coupled thermo-hydro-mechanical math model was developed on the basis of Fickian diffusion theory, Fourier's law of heat conduction and thermoelasticity mechanics in order to analyze the spatio-temporal distributions of moisture, temperature and drying stresses in the potatoes. The transient mathematical model, composed of a system of partial differential equations, was solved by finite difference methods. The numerical results obtained by using the mathematical model were in good agreement with the experimental data. The variations in temperature and moisture distributions, drying curves and stresses within potatoes over time were simulated, and the ways in which these are affected by the drying conditions were discussed. This work could help in developing an understanding of the relationship between mass and heat transfer, shrinkage, stress, and physical degradation of biological materials.

Keywords: heat and mass transfer, deformable porous media, THM coupling, mathematical modeling
DOI: 10.3965/j.ijabe.20160905.2057

Citation: Wang H L, Lu T, Zhang Q G. Drying characteristics of biological porous media during convective drying. Int J Agric & Biol Eng, 2016; 9(5): 194－207.

1 Introduction

Most of the foodstuffs have been modeled as porous media[1]. Drying is an operation evacuating the solvent (water or others) that exists in void (pore) spaces. This process offers advantages in terms of storage, transportation and second time procession of food products. It has been shown to be a complex phenomenon in which heat and mass transfer occur simultaneously[2-5] accompanied by biological tissue shrinkage[6-9]. Investigation of the drying behaviour is important for enhancing our understanding of the overall drying process.

Experimental study of drying process of agriculture product has been carried out by some researchers[5,10,11]. The results obtained included not only in the aspect of the reliable drying kinetics and thermal behaviour under different drying conditions, but also in the visual observation of the shrinkage of the product during drying, which provided important data for the predictive drying models. Simulation of the temperature and moisture distributions during the drying process was studied by many researchers in recent years[3,5,12-15]. In these studies, Fourier's law of heat conduction and Fick's second law of diffusion were coupled to control the heat and moisture transportation. Researchers have employed numerical computing methods to study moisture and temperature distributions within porous media and compared their calculations with the experimental data available for certain drying conditions,

Received date: 2015-07-14 **Accepted date:** 2016-01-03
Biographies: Wang Huilin, PhD, Lecturer, research interest: heat and mass transfer, Email: whl-410@163.com; **Zhang Quanguo,** PhD, Professor, research interest: biomass energy, Email: zquanguo@163.com.

***Corresponding author: Lu Tao,** PhD, Professor, research interest: engineering thermophysics. Mailing address: No. 15, North Third Ring Road, Chaoyang District, Beijing 100029, China. Tel: +86-10-64417994, Email: likesurge@sina.com.

while the analytical models employed simplified approaches, i.e., shrinkage or deformation of the porous solid frame was neglected in above-mentioned modeling studies. Since this is one of the main parameters governing the drying process, it is desirable to take it into account when predicting drying characteristics for convective drying of deformable porous media. In fact, recent experimental and theoretical studies have demonstrated the importance of considering shrinkage in order to give a more realistic analysis of drying phenomena[7,9,15-19]. For this purpose, different types of models have been used to predict the length contraction and volume change of deformable porous media. Some researchers suggested that the experimental changes in (L/L_0) and (V/V_0) can be represented, respectively, as a linear function and a logarithmic function of the varying moisture content[7,9]. A second-order polynomial relationship between volume changes and moisture content of the samples during the drying process was also proposed[15,19]. The correlations between volume changes and moisture content were fitted for various drying conditions such as operating temperature and air velocity for a variety of samples. In an attempt to improve the generality of the conclusions, mechanisms of free shrinkage strains in desiccating deformable porous media were also studied based on stress and strain relations[16,20,21]. They analyzed the internal stress distribution during the drying process by solving the fundamental equations of stress and strain, and showed that this is a more realistic way to describe the drying process of porous media. However, by calculating the one-way coupling of the deformation with the heat and mass transfer equations, they only considered the influence of heat and moisture distribution on the stress and strain and ignored the influence of the deformation on the heat and mass transfer during the drying process, and it was unable to obtain a detailed understanding of the drying process.

Lu T, et al.[22,23] studied preliminarily on the deformation of porous media during hot air drying. Based on the above efforts, the objective of this work was to analyze the processes of heat and mass transfer two-way coupled with the deformation of porous media during drying. In order to give a complete description of the process, a transient mathematical model involving two-phase model equations for heat and mass transfer with thermodynamic equilibrium between the phases coupled two-way sequentially with stress equilibrium equations was solved by finite difference methods. The validity of the mathematical model was assessed by comparison with experimental data from the drying of potatoes. Furthermore, the temporal-spatial variation of stress (normal stress and shear stress) in the potato during drying and their affected ways by the drying conditions were discussed.

2 Numerical survey

2.1 Physical modeling

The system under study is shown in Figure 1. The following assumptions were made in order to write two-dimensional thermo-hydro-elasticity equations, and unsteady energy and mass equations:

(1) The biological porous medium is homogeneous and isotropic;

(2) The deformation during drying is elastic[24];

(3) The porous medium and drying air have constant density and thermal conductivity;

(4) Heat and mass transfer within the product is governed by diffusion, and that between the material and the air is governed by convection;

(5) Critical moisture content can be used as a judgment standard for dry and wet zones[25].

2.2 Mathematical model

2.2.1 Basic thermo-hydro-elasticity equations

According to assumption (2), the porous medium undergoes elastic deformation during the drying process, the basic elasticity equations applicable to heat and humidity include the balance equations, the geometric equations and the constitutive equations[26]. The volume force is zero regardless of the external load.

The equilibrium differential equations for a planar problem can be expressed as:

$$\frac{\partial \sigma_{xx}}{\partial x}+\frac{\partial \tau_{xy}}{\partial y}=0 \tag{1}$$

$$\frac{\partial \tau_{yx}}{\partial x}+\frac{\partial \sigma_{yy}}{\partial y}=0 \tag{2}$$

where, σ_{xx} and σ_{yy} are normal stress, Pa; τ_{xy} and τ_{yx} are shear stress, Pa.

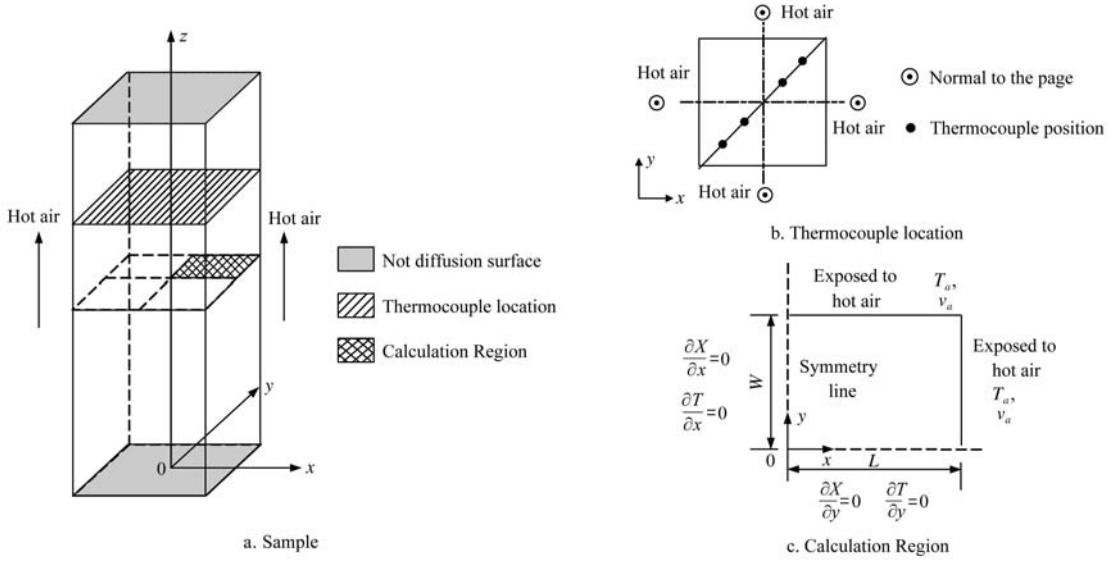

Figure 1 The system under study

The geometric equations for a planar problem can be expressed as:

$$\varepsilon_{xx}=\frac{\partial d_x}{\partial x} \tag{3}$$

$$\varepsilon_{yy}=\frac{\partial d_y}{\partial y} \tag{4}$$

$$\varepsilon_{xy}=\frac{1}{2}\left(\frac{\partial d_x}{\partial y}+\frac{\partial d_y}{\partial x}\right) \tag{5}$$

where, ε_{xx} and ε_{yy} are normal strain; ε_{xy} is shear strain; d_x and d_y are displacement of solid skeleton.

Considering thermal and humidity effects, the elastic strain in the porous medium can be expressed as the sum of two parts: one part is due to the changes in temperature and moisture content, and the strain ε^T and ε^H induced by free expansion or free shrinkage at each point of the medium; the other part, ε^M, is due to the mutual constraints on the parts of the elastic body. Therefore, the total strain is expressed as:

$$\varepsilon=\varepsilon^M+\varepsilon^T+\varepsilon^H \tag{6}$$

Since, according to assumption (1), the porous medium is isotropic, the strain induced by heat and humidity should also be isotropic, namely the linear strain caused by compression and elongation at a point is the same in each direction, and there is no shear strain. If the variations in temperature and moisture content at one point in the porous medium between the current time and the initial time are respectively ΔT and ΔX, and the thermal and humidity expansion coefficients are respectively α and β, the strain tensors ε^T, ε^H can be expressed as[21]:

$$\varepsilon^T=\alpha(T-T_0)=\alpha\Delta T \tag{7}$$

$$\varepsilon^H=\beta(X-X_0)=\beta\Delta X \tag{8}$$

The constitutive equations for the porous media are different from the equations under isothermal conditions. The constitutive equations, taking into account thermal and humidity effects, can be expressed as:

$$\sigma_{xx}=\lambda(\varepsilon_{xx}+\varepsilon_{yy})+2G\varepsilon_{xx}-3K\alpha(T-T_0)-3K\beta(X-X_0) \tag{9}$$

$$\sigma_{yy}=\lambda(\varepsilon_{xx}+\varepsilon_{yy})+2G\varepsilon_{yy}-3K\alpha(T-T_0)-3K\beta(X-X_0) \tag{10}$$

$$\tau_{xy}=2G\varepsilon_{xy} \tag{11}$$

where, λ and G are bulk modules and shear modules of elastic deformation, Pa; K is modulus of volume elasticity, Pa.

2.2.2 Mass conservation equation

Based on Fickian diffusion theory and the continuity equation, by considering the influence of the deformation of the porous solid frame during the drying process and ignoring the influence of pore water vapor, the mass transfer model describing the dry basis moisture content in a biological porous medium can be derived as follows[27]:

For the solid:

$$\frac{\partial\rho_s}{\partial t}+u_s\frac{\partial\rho_s}{\partial x}+v_s\frac{\partial\rho_s}{\partial y}=0 \tag{12}$$

where, ρ_s is volume density, kg/m^3; t is time, s; u_s, v_s are solid velocity, m/s. The solid velocity is assumed to be

equal to the product velocity at any point:

$$u_s = \frac{\partial d_x}{\partial t} \tag{13}$$

$$v_s = \frac{\partial d_y}{\partial t} \tag{14}$$

When $X \geq X_{cr}$, for the liquid:

$$\frac{\partial \rho_l}{\partial t} + u_l \frac{\partial \rho_l}{\partial x} + v_l \frac{\partial \rho_l}{\partial y} = 0 \tag{15}$$

When $X < X_{cr}$, for the liquid:

$$\frac{\partial \rho_l}{\partial t} + u_l \frac{\partial \rho_l}{\partial x} + v_l \frac{\partial \rho_l}{\partial y} + \dot{m}_v = 0 \tag{16}$$

where, ρ_l is volume density, kg/m^3; u_l, v_l are liquid velocity, m/s.

And,

$$\rho \vec{v} = \rho_s \vec{v_s} + \rho_l \vec{v_l} \tag{17}$$

$$\rho = \rho_s + \rho_l \tag{18}$$

Moreover, the mass flux can be decomposed into terms involving diffusion and convection:

$$\rho_l \vec{v_l} = \overrightarrow{J_{D,l}} + \rho_l \vec{v} \tag{19}$$

where, $\overrightarrow{J_{D,l}}$ is liquid diffusion flux (kg/m^2·s):

$$\overrightarrow{J_{D,l}} = -D_{eff} \left(\frac{\partial \rho_l}{\partial x} \vec{i} + \frac{\partial \rho_l}{\partial y} \vec{j} \right) \tag{20}$$

The dry basis moisture content X (kg/kg d.b.) is defined as the ratio of the volume densities of the two phases (liquid and solid):

$$X = \frac{\rho_l}{\rho_s} \tag{21}$$

Combining Equations (12) to (21), the liquid transport equation for the wet zone takes the final form:

$$\frac{\partial X}{\partial t} + u_s \frac{\partial X}{\partial x} + v_s \frac{\partial X}{\partial y} = D_{eff} \left(\frac{\partial^2 X}{\partial x^2} + \frac{\partial^2 X}{\partial y^2} \right) \tag{22}$$

The liquid transport equation for the dry zone takes the final form:

$$\frac{\partial X}{\partial t} + u_s \frac{\partial X}{\partial x} + v_s \frac{\partial X}{\partial y} = D_{eff} \left(\frac{\partial^2 X}{\partial x^2} + \frac{\partial^2 X}{\partial y^2} \right) - \frac{\dot{m}_v}{\rho_s} \tag{23}$$

where,

$$\dot{m}_v = \phi \frac{\partial \rho_v}{\partial t} + u_s \frac{\partial \rho_v}{\partial x} + v_s \frac{\partial \rho_v}{\partial y} - D_{vs} \left(\frac{\partial^2 \rho_v}{\partial x^2} + \frac{\partial^2 \rho_v}{\partial y^2} \right) \tag{24}$$

where, D_{eff} is effective diffusion coefficient, m^2/s; $\dot{m}_v$ is volume rate of moisture vaporization, kg/m^3·s; ϕ *is* porosity; D_{vs} is water vapor diffusion coefficient, m^2/s.

2.2.3 Energy conservation equation

In the process of drying at constant speed, moisture evaporation occurs only on the surface of the porous medium. Heat conduction inside the porous medium obeys Fourier's law, and together with the energy removed by liquid diffusion and heat transfer due to deformation of the solid skeleton, the heat transfer equations can be expressed as Equation (25) for the wet zone.

$$\frac{\partial (\rho C_p T)}{\partial t} = \kappa \left(\frac{\partial^2 T}{\partial x^2} + \frac{\partial^2 T}{\partial y^2} \right) + \frac{D_{eff}}{1+X} (\rho C_p) \left(\frac{\partial X}{\partial x} \frac{\partial T}{\partial x} + \frac{\partial X}{\partial y} \frac{\partial T}{\partial y} \right) - \left(u_s \frac{\partial (\rho C_p T)}{\partial x} + v_s \frac{\partial (\rho C_p T)}{\partial y} \right) \tag{25}$$

where, C_p is heat capacity, J/kg·K; κ *is* thermal conductivity, W/m·K. In the process of drying at falling rate stage, the interface of moisture evaporation back to the internal porous media, the bound water in dry zone turns it into vapor in form of local evaporation, hence, the heat transfer equations can be expressed as Equation (26) for the dry zone:

$$\frac{\partial (\rho C_p T)}{\partial t} = \kappa \left(\frac{\partial^2 T}{\partial x^2} + \frac{\partial^2 T}{\partial y^2} \right) + \frac{D_{eff}}{1+X} (\rho C_p) \left(\frac{\partial X}{\partial x} \frac{\partial T}{\partial x} + \frac{\partial X}{\partial y} \frac{\partial T}{\partial y} \right) - \left(u_s \frac{\partial (\rho C_p T)}{\partial x} + v_s \frac{\partial (\rho C_p T)}{\partial y} \right) - \dot{m}_v L_v \tag{26}$$

The physical meaning of Equation (25) is that the increasing energy per unit volume per unit time in the porous medium constraining the bound water (the left-hand side of the equation) is equal to the energy associated with nearby heat conduction (the first term on the right-hand side of the equation) plus the energy associated with the diffusion of liquid water (the second term on the right-hand side of the equation) minus the energy associated with the solid displacement (the third term on the right-hand side of the equation). Removing the energy of liquid water local evaporation from Equation (25) leads to Equation (26) for the dry zone.

2.3 Deterministic conditions of the solution

2.3.1 Deterministic conditions of basic thermo-hydro-elasticity equations

The initial conditions and boundary conditions for the stress equilibrium equations are:

at $0 \leq x \leq L$, $y = 0$:

$$d_y = 0, \quad \frac{\partial d_x}{\partial y} = 0 \tag{25}$$

at $x=L$, $0\le y\le L$:

$$\sigma_{xx}=0,\ \ \tau_{xy}=0 \tag{26}$$

at $0\le x\le L$, $y=W$:

$$\sigma_{yy}=0,\ \ \tau_{xy}=0 \tag{27}$$

at $x=0$, $0\le y\le W$:

$$d_x=0,\ \ \frac{\partial d_y}{\partial x}=0 \tag{28}$$

2.3.2 Deterministic conditions of heat and mass transfer equations

The initial conditions for the mass and energy conservation equations are:

at $t=0$,

$$X=X_0 \text{ and } T=T_0 \tag{29}$$

where, X_0 and T_0 are initial value.

The boundaries of wet and dry zones are shown in Figure 2.

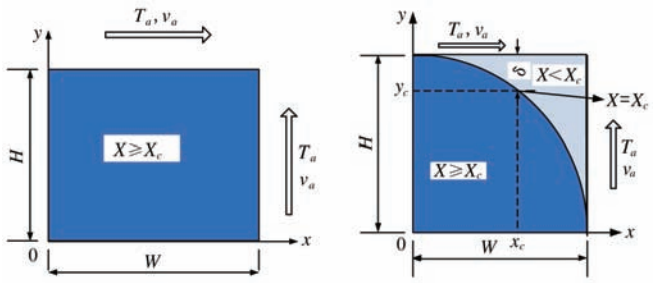

a. Wet zone b. Dry zone

Figure 2 Boundary conditions

The boundary conditions for the mass and energy conservation equations are:

at $0\le x\le L$, $y=0$:

$$\frac{\partial X}{\partial y}=0,\ \ \frac{\partial T}{\partial y}=0 \tag{30}$$

at $x=0$, $0\le y\le W$:

$$\frac{\partial X}{\partial x}=0,\ \ \frac{\partial T}{\partial x}=0 \tag{31}$$

When $X_s\ge X_{cr}$, the whole calculation region is wet zone, see Figure 2a, hence, the boundary conditions for the mass and energy conservation equations of wet zone are:

at $x=L$, $0\le y\le W$:

$$\dot{m}_s=-\rho_s D_{eff}\frac{\partial X}{\partial x};\ \ h(T_a-T_{surf})=(\dot{m}_s L_v(T_{surf}))+\kappa\frac{\partial T}{\partial x} \tag{32}$$

at $0\le x\le L$, $y=W$:

$$\dot{m}_s=-\rho_s D_{eff}\frac{\partial X}{\partial y};\ \ h(T_a-T_{surf})=(\dot{m}_s L_v(T_{surf}))+\kappa\frac{\partial T}{\partial y} \tag{33}$$

where, $\dot{m}_s$ is surface rate of moisture vaporization in wet zone, kg/m^2·s; T_a and T_{surf} are temperature of air and medium surface, K; $L_v(T_{surf})$ is latent heat of evaporation, kJ/kg.

$$\dot{m}_s=\frac{h_m M_v}{R}\left(\frac{a_w\times P_{v,sat\ at\ T}}{T}-\frac{RH\times P_{v,sat\ at\ T_a}}{T_a}\right) \tag{34}$$

In Equation (34), h_m is mass transfer coefficient between the product and air in wet zone, m/s; M_v is molecular weight of water, kg/kmol; R is universal gas constant, J/kmol·K; $P_{v,sat\ at\ T}$ and $P_{v,sat\ at\ Ta}$ are saturated steam pressure at the temperature of T and T_a, Pa; RH is relative humidity, %; a_w is the water activity as function of moisture. However, the value of a_w is close to 1 in the high water content of food materials (greater than 1 kg/kg d.b.). Equation (38) is the interface mass transfer of wet zone, where, dry basis moisture content of potato was higher than 1 kg/kg d.b.

When $X_s<X_{cr}$, the calculation region is divided into wet zone and dry zone, see Figure 2b, hence, the boundary conditions for the mass and energy conservation equations of dry zone are:

at $x=L$, $0\le y\le W$:

$$\dot{m}_s^*=-\rho_s D_{eff}\frac{\partial X}{\partial x};\ \ h(T_a-T_{surf})=\kappa\frac{\partial T}{\partial x} \tag{35}$$

at $0\le x\le L$, $y=W$:

$$\dot{m}_s^*=-\rho_s D_{eff}\frac{\partial X}{\partial y};\ \ h(T_a-T_{surf})=\kappa\frac{\partial T}{\partial y} \tag{36}$$

where, $\dot{m}_s^*$ is surface rate of moisture vaporization in dry zone (kg/m^2·s):

$$\dot{m}_s^*=h_m^*(X_s-X_e) \tag{37}$$

where, h_m^* is mass transfer coefficient between the product and air in dry zone, m/s.

The boundary of the interface of the wet zone and the dry zone is made up by all these points (x_c, y_c), where the dry basis moisture content equal to the critical moisture content, and the boundary conditions for the interface are controlled by the equations as with the wet zone except for the difference that $\dot{m}_s$ is replaced with $\dot{m}_i$, T_{surf} is replaced with T_{x_c,y_c} and T_a is replaced with the temperature of grid nodes in dry zone which are next to

points (x_c, y_c):

Where,

$$\dot{m}_i = \frac{D_{vs}}{\delta}(\rho_v - \rho_{v,e}) \tag{38}$$

Since Reynolds numbers of cases 1-5 (in section 3.2) in this study were between 940 and 3000, which were all less than the critical Reynolds number (5×10^5), the values of the heat transfer coefficient h (W/m^2·K) and mass transfer coefficient h_m (m/s) were calculated according to the following formulas:

$$h = 0.664\frac{\kappa}{H}Re^{0.5}Pr^{0.33} \tag{39}$$

$$h_m = 0.664\frac{D_{va}}{H}Re^{0.5}Sc^{0.33} \tag{40}$$

where, Re, Pr and Sc are Reynolds number; Prandtl number and Schmidt number.

The values of the physical and mechanical properties of potatoes were related to the previous research of authors[22,23].

2.4 Numerical solution

Parameters such as temperature, moisture content and displacement can be a function of the space domain and the time domain. The explicit finite difference method was used for the time term and the central difference scheme was used for the space term in the numerical resolution of the model. The bidirectional coupling process between heat and mass transfer equations and the stress and strain equations was proceeding as follows:

(1) Seting up the computational domain, dividing the grids accordingly;

(2) Calculating the heat and mass transfer parameters on all mesh points according to the initial conditions and drying conditions;

(3) Selecting wet zone model or dry zone model by comparing the scale of dry basis moisture content and critical dry basis moisture content;

(4) Calculating the value of "X" and "T" on all mesh points according to the mass and energy conservation equations at that time t, and stresses would be generated by the uneven distribution of the moisture content and temperature;

(5) Calculating the value of average dry basis moisture content, if less than the equilibrium moisture content, numerical procedures ended, then going to step (6);

(6) Pluging the latest calculated value of "X" and "T" into stress balance equations, calculating the value of "d_x", "d_y", "σ", "τ" and "ε" of biological porous media, the displacement of porous media should affect the distribution of the moisture content and temperature at next time step;

(7) Pluging the latest calculated value of "d_x" and "d_y" into coupled heat and mass transfer equations; going back to step (3) to begin a new cycle.

3 Meterials and methods

3.1 Experiment setup

A convective hot air dryer was used for drying, and could be regulated to restrict the air temperature and velocity of the drying air within certain limits with high accuracy. The principal components involved in the drying process are a centrifugal blower to aspire the ambient air, a vortex-shedding flowmeter (LUGB DN80, Beijing flowmeter, China) to measure the air velocity, an air heater to raise the temperature of the air, a heating control unit, a damping screen and a drying chamber (Figure 3).

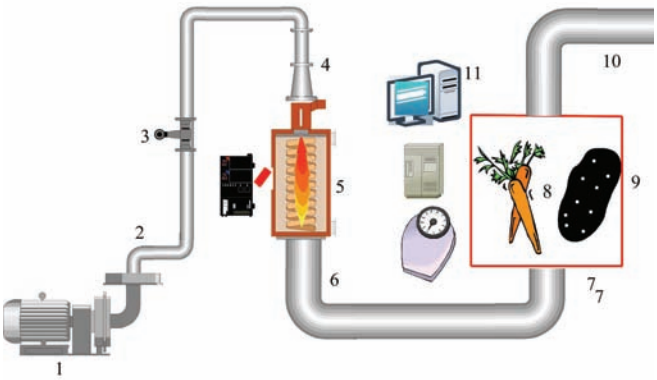

1. Air blower 2. Connecting line 3. Vortex-shedding flowmeter 4. Connecting line before the heater 5. Heater 6. Connecting line after the heater 7. Damping screen 8. Biological porous medium 9. Drying section 10. Exhaust pipe 11. Data collection system

Figure 3 Flow chart of the drying process

The orientation of the hot air was vertical on the samples. The air temperature and velocity inside the vein were adjusted and controlled using an automatic regulation system. The humidity ratio of the air was not controlled, but calculated from the dry bulb temperatures and the relative humidity as measured by a

thermohygrograph. The weight of the potato slab was measured using a high precision analytical balance (ME204, Mettler toledo, Swiss). The temperature was measured using thermocouples, and the analogue signals generated by the thermocouples were converted to temperature by using a data acquisition system (AGILENT 34970A, Agilent Technologies, China). The length and width of the potato slab were measured using a dial micrometer.

3.2 Experiment procedure

Fresh potatoes were purchased from a local market (Beijing, China). Before drying, the potatoes were peeled, cut into samples with a size of 20 mm×20 mm×40 mm (thickness×width×length), and placed in water at 15°C for about 15 min to preventing loss of sample through evaporation if exposed in the air. Before the experiments, the remaining surface water was removed with a filter paper. In order to ensure that the internal moisture underwent two-dimensional diffusion, the two sides of the samples in the z direction were covered with a thin epoxide-resin glue film in order to make them waterproof (see Figure 1a). Finally, the samples were hung on a stainless steel wire hook on a beam. The beam was suspended in the drying chamber, as shown in Figure 3. The mass changes of the product were measured at five-minute intervals during the first hour of drying and then at 20-minute intervals. Thermocouples were placed inside the potato to measure the temperature (see Figure 1b). The drying tests were terminated when the mass of the samples reached a constant value. Also, in order to evaluate the shrinkage behaviour of the product, measurements of length and width were made at two different positions on each sample each time they were removed for weighing. The moisture content dry basis of the product was determined after each experiment by drying on a hot stove at 80°C for 48 h. The initial moisture content varied between 4 and 4.5 kg/kg d.b. The different drying conditions tested are listed in Table 1: the temperature and the velocity of the drying air ranged from 70°C to 90°C and 0.5 m/s to 1.5 m/s, respectively. The experimental data were processed as follows:

The dry basis moisture content of the potato (X) was calculated using[28]:

$$X = \frac{M_t - M_d}{M_d} \tag{41}$$

where, M_t is sample mass at time t, kg; M_d is dry mass of sample, kg.

The drying rate (U) was calculated using[28]:

$$U = \frac{M_d \times dX}{A \times dt} \tag{42}$$

where, A is total drying surface of sample, m^2.

The retention rate (r) of the sample was calculated using:

$$r = \frac{L_x}{L_{x0}} \tag{43}$$

where, L_x is current length of sample; L_{x0} is initial length of sample.

Table 1 Experiment conditions

Case	Moisture content of air /g·kg^{-1}	Temperature of the heater /°C	Air velocity /m·s^{-1}	Relative humidity /%	Wet bulb temperature of hot air/°C
1	9.56	70	1	7.69	27.53
2	8.224	80	0.5	4.24	29.04
3	8.734	80	1	4.5	29.31
4	7.891	80	1.5	4.07	28.86
5	8.513	90	1	2.85	31.30

4 Results and discussion

4.1 Experimental drying results

Drying conditions such as air temperature and air velocity are important factors influencing drying curves. The representative results for the convective drying process are shown in Figure 4 and Figure 5. The influence rule of drying conditions on drying curves in this study agree well with the literature data[29,30]. The drying rate increases with the increasing of air temperature and velocity, because the increase in the heat flux transmitted by air to the product, and the acceleration of the internal water migration associated with the increasing coefficient of diffusion. Drying kinetics of potatoes obtained under different conditions involve either a very short constant drying rate period or no constant rate drying period, and the drying process takes place entirely-or almost entirely-during the period of falling drying rate. This is consistent with the literature, where drying of biological products is most commonly reported to occur in the falling rate period.

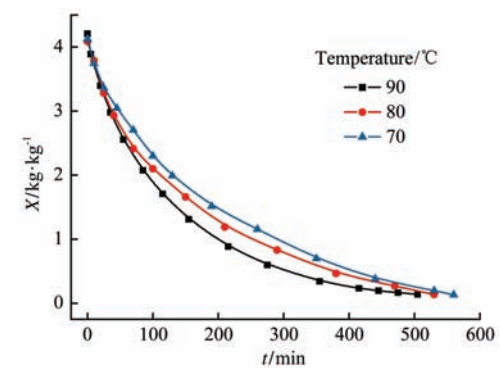

a. Moisture content

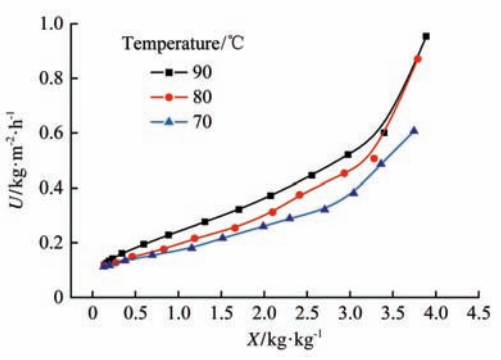

b. Drying rate

Figure 4 Drying curves at velocity v_a=1 m/s

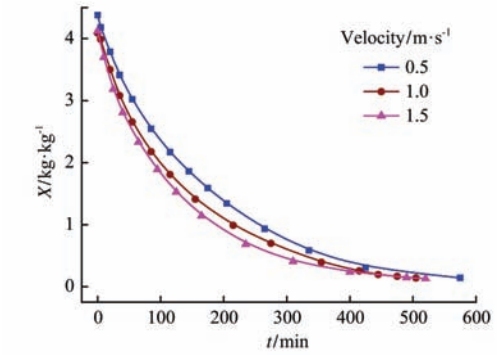

a. Moisture content

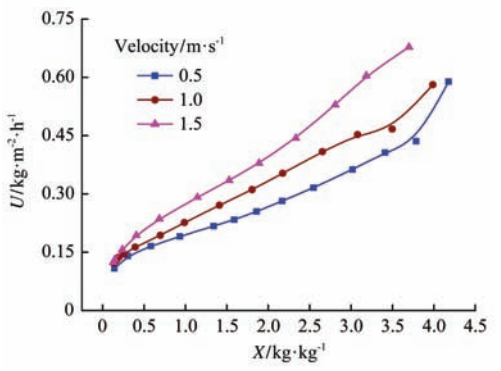

b. Drying rate

Figure 5 Drying curves at 80°C

Figure 6 shows the structural changes observed in potato samples dried for different times with an air velocity of 1 m/s and air temperature of 80°C. Figure 6 shows that shrinkage deformation takes place throughout the whole drying process, and the deformation behavior of potato shows a significant variation with time. At 106 min (Figure 6a), an obvious deformation of the potato is already appeared. At 186 min (Figure 6b), deformation is not uniform from the surface to the center either horizontally or vertically, and the middle parts of the potato become invaginated in the vertical direction. This is because the upper surface and the lower surface of the potato sample were covered by epoxide-resin glue to make them waterproof, and the wrinkling of the potato surface in the horizontal direction is caused by the drying stress induced by the inconsistent moisture content gradient within the potato sample during drying. At 306 min (Figure 6c) and 386 min (Figure 6d), it can be seen that the invagination and wrinkling become even more pronounced.

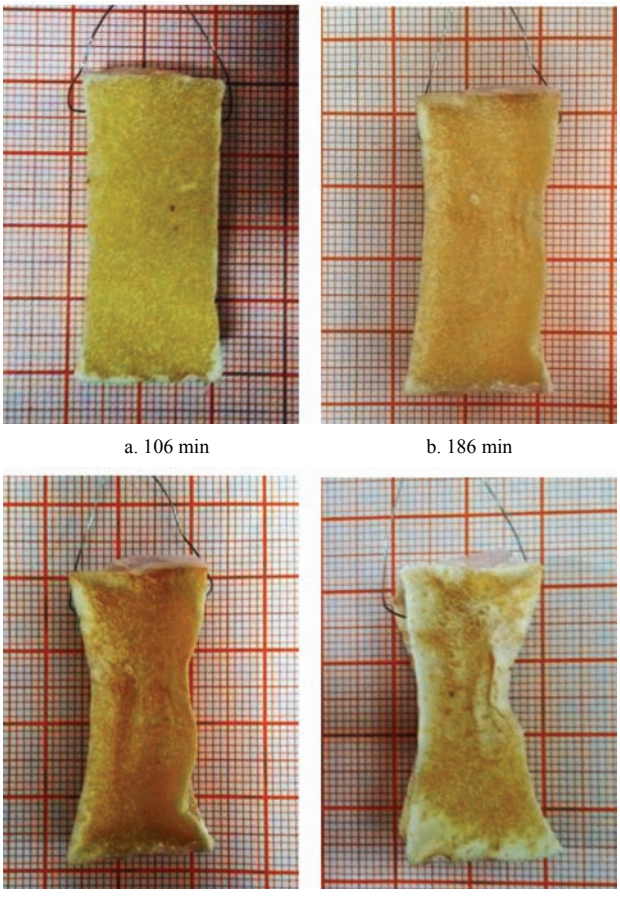

a. 106 min b. 186 min

c. 306 min d. 386 min

Note: The smallest division on the graph paper: 1 mm; air velocity: 1 m/s, air temperature: 80°C.

Figure 6 Structure changes during convective drying of potatoes

4.2 Validation of the model

In order to check the validity of the mathematical model and numerical simulation results, the experimental drying data for case 3 were compared with the model. The experimental conditions are listed in Table 2, with an

initial moisture content of 4.09 kg/kg d.b. and an initial temperature of 15°C. Figure 6 shows the experimental and theoretical results for the variation in the average dry basis moisture content and internal temperature over time.

It can be seen in Figure 7a that the theoretic results and experimental data for the average dry basis moisture content agree reasonably well, with the relative errors between them being less than 5%. In Figure 7b, the simulation temperature was higher than actual temperature most of the drying time, and it seemed that the actual temperature and theoretical temperature did not fit well. However, 98.4% of the relative errors between the theoretical results and the temperature data collected during drying process which were more than three thousand were less than 20%, which were in an acceptable range. This showed that the mathematical model had some deficiencies in predicting inner-temperature of potatoes, and it still had much room to be improved in the future study. As shown in Figure 6b, the theoretical and experimental data for the changes in internal temperature over time also show the same qualitative trends.

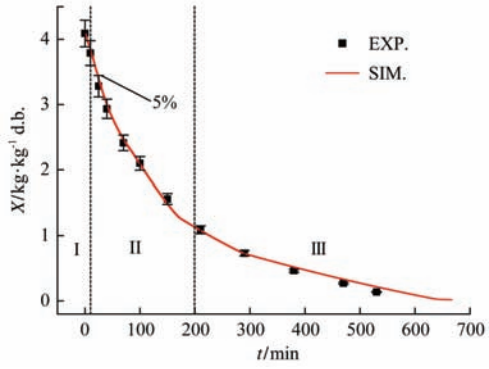

a. Moisture content

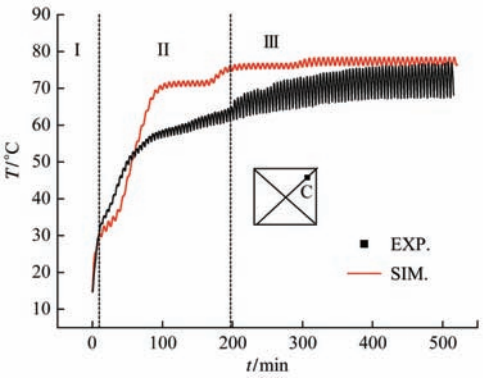

b. Temperature

Note: air velocity: 1 m/s, air temperature of 80°C.

Figure 7 Average dry basis moisture content and temperature change over time for experiments and simulation

The temperature of the measurement point inside the potato increased to the wet bulb temperature of the hot air in the first nine minutes after the drying starting. The average dry basis moisture content fell rapidly, according to the balance relationship between the latent heat of evaporation and heat of convection heating. This initial period is denoted the constant speed drying stage (Figures 7a and 7b). From 9-200 min, part of the energy from convection heating was used to heat the sample and the temperature started to rise rapidly above the wet bulb temperature. The remainder of the convection heat energy was employed in water evaporation, and the decrease rate of the average dry basis moisture content slowed down over this period. This second stage is known as the first falling-rate drying period (Figures 7a and 7b). After 200 min drying, the temperature reached a high level near to the hot air temperature, and then increased only slightly and the rate of average dry basis moisture content changed slowly over time. This third stage is known as the second falling-rate drying period (Figures 7a and 7b). The whole drying process can thus be divided into the three stages, which is consistent with the typical drying curves for porous absorbent materials[28], and this further demonstrates the credibility of both experimental data and simulation results.

Figure 8 shows the simulated deformation and moisture distribution at different times. Deformation in the x and y directions is different and the moisture distribution shows a gradient during drying.

Figure 9 shows the relation schema for r with dry basis moisture content both experimental data and simulation results. Experiments[31] on mechanical properties of biological porous media showed some biological tissues like potatoes were viscoelastic body, their rheological performance parameters would be ascertained by stress relaxation test. Potatoes were both viscous and elastic properties with higher moisture content (4.5-1 kg/kg d.b.). The viscous property gradually disappeared along with moisture content decreasing during drying. However, the mechanical properties was defined as a constant in this study which should be as a function of moisture content.

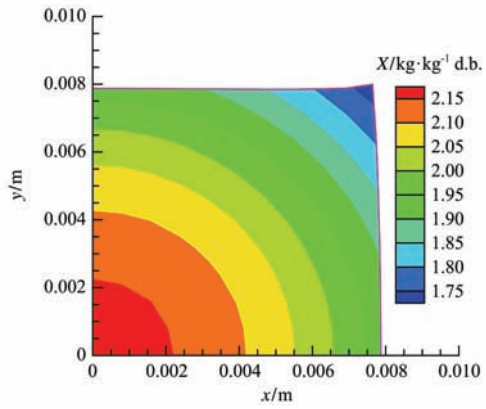

a. 106 min

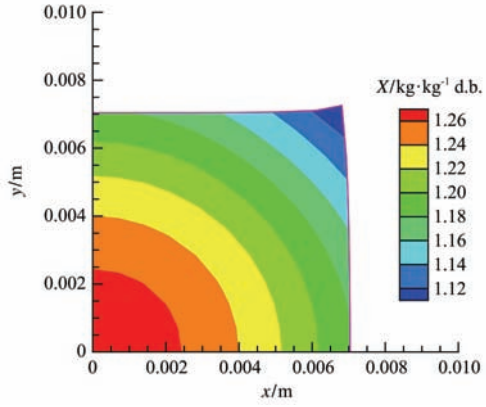

b. 186 min

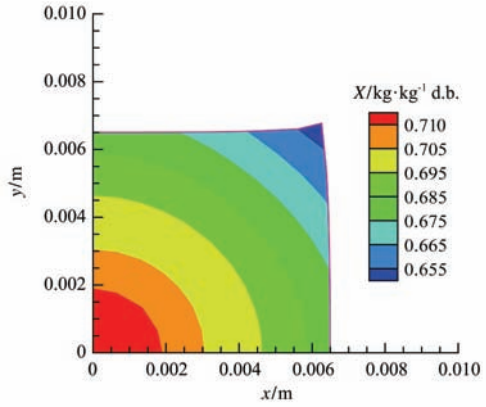

c. 306 min

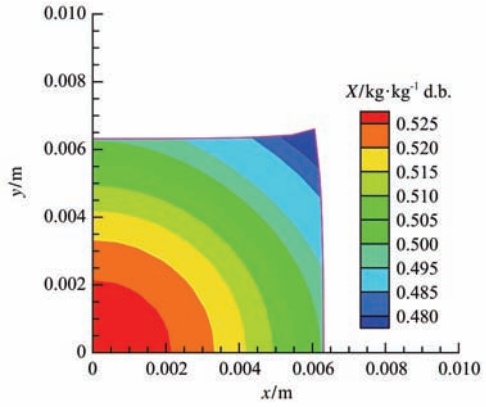

d. 386 min

Note: air velocity: 1 m/s, air temperature: 80°C.

Figure 8 Deformation and moisture distribution of potatoes at different times

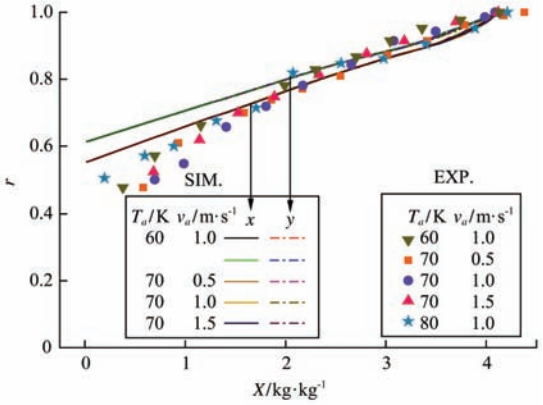

Figure 9 Relation schema for r with dry basis moisture content for both experimental data and simulation results

Therefore, it can be seen in Figure 9 that when the experimental change in average dry basis moisture content reached about 1 kg/kg d.b., the theoretical results did not agree well with the experimental data. This discrepancy can be explained in terms of the change in mechanical properties of the potato during drying. Both the experimental data and simulation results show that the deformation is determined by the average dry basis moisture content and is unrelated to the drying conditions.

4.3 Numerical results

4.3.1 Effect of relative humidity on drying rate

In addition to air temperature and air velocity, relative humidity is also an important factor influencing drying curves. Although it was not possible to carry out an experimental single factor analysis for relative humidity due to limitations in our apparatus, the numerical simulations of a single factor analysis for relative humidity were performed with an air temperature of 80°C and an air velocity of 1 m/s.

The influence of relative humidity on the drying curves is shown in Figure 10. When the relative humidity of the air decreased, the drying rate in the first and second drying stages increased because the lower relative humidity increased the mass transfer coefficient between the air and the potato sample. In contrast, however, changing the relative humidity in the third drying stage had little effect on the drying rate. This is because the moisture content inside the potato was relatively low in the third drying stage. It was found that the average dry basis moisture content first increased to slightly more than the initial value and subsequently

fell (Figure 10a), and the drying rate therefore changed from negative to positive at the start of drying (Figure 10b). This can be attributed to the condensation of water vapor in the hot air on the sample, because the temperature of the sample surface was lower than the dewing temperature of the hot air. The same effect was also found by Yu[25] in their modeling of the drying of wood.

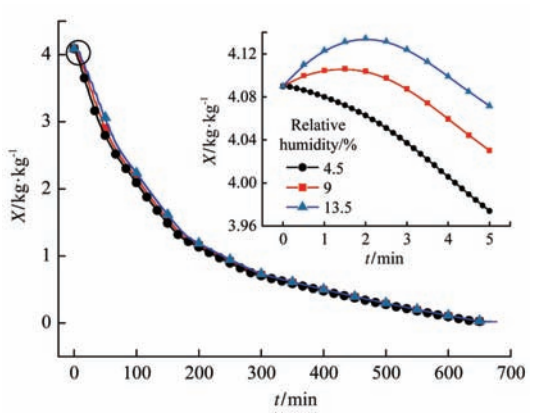

a. Moisture content

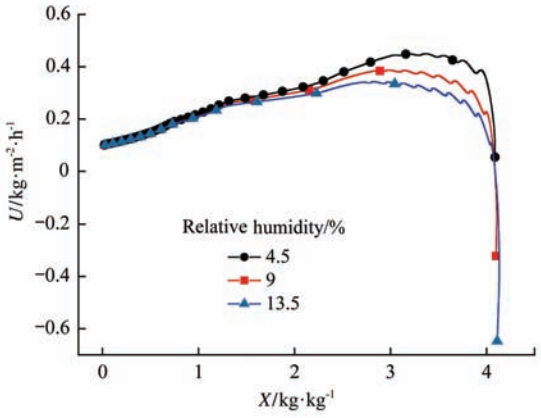

b. Drying rate

Figure 10 Drying curves at different relative humidities (T_a=80°C, v_a=1 m/s)

4.3.2 Drying stress

Drying stress is induced due to the deformation of potato during drying. Figure 11 shows the temporal variation of stress (normal stress and shear stress) in the potato at some nodes during the drying conditions for case 3 (see Table 1). The stresses of five points (point A, point B, point C, point D and point E) in calculation region were analyzed, and analysis of the normal stress shows that during most of the drying time, to the points A, B and C from which they are equal in the direction to the heat-and mass-transferring surfaces, the type of stresses that the porous media must withstand during drying were compressive stress in all directions, but to the point D and point E from which they are not equal in the direction to the heat-and mass-transferring surfaces, the type of stresses were different from the previous ones: at point D which is nearer to the upper heat-and mass-transferring boundary (see Figure 2), the type of stresses were tensile stress in the x direction; at point E which is nearer to the right heat-and mass-transferring boundary (see Figure 2), the type of stresses were tensile stress in the y direction. In addition, the normal stresses were null at zero time because the initial moisture content distribution of the sample was uniform. As the drying process proceeded, the normal stresses began to increase gradually because the temperature and a moisture gradient both appeared in the material and increased gradually. Subsequently, the normal stresses increased rapidly and reached its maximum value. This rapid increase can be attributed to the rapid decrease in moisture content. Finally the normal stresses began to decrease because moisture content gradually became more evenly distributed, and the values in x and y direction tended to become similar. The variations in shear stress over time were qualitatively similar to those of the normal stresses, but the values for shear stresses were found to be much lower than those for the normal stresses. Similar observations were also found by Mezhericher et al.[32] and Arrieche et al.[33] in the modeling of particle breakage during drying of a spherical foodstuff.

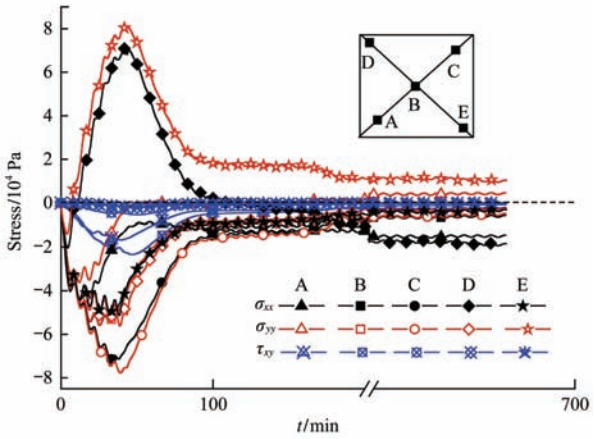

Figure 11 Temporal variation of the stress in the potato at some nodes under drying conditions of Case 3

Figure 12 shows the spatial variation of stress (normal stress and shear stress) in the potato under the drying conditions for Case 3 (see Table 1) at the end of drying. The distributions of normal stress σ_{xx} and σ_{yy} in the x

direction are shown in Figures 12a and 12b, respectively. As shown in Figure 12a, the value of σ_{xx} was zero at x/x_{max}=1, where it is a free boundary, whereas they were negative in other parts of the material, which means they are subjected to compressive stresses in the direction of moisture diffusion. This may be the reason why the potato surface wrinkled in the horizontal direction (see Figure 6), as discussed elsewhere in connection with the formation of a folded mountain[34]. The simulated normal stress σ_{yy} values in the x direction changed from negative to positive on going from x/x_{max}=0.5 to x/x_{max}=0.7, as shown in Figure 12b. This implies that the potato was compressed close to its center and under tension near its boundary surface, which causes an irregular deformation of the potato (see Figure 6). The shear stress τ_{xy} distribution in the x direction is shown in Figure 12c. Careful comparison of the two stresses shows up some key differences and similarities, with the main difference being that the values of shear stress were not as large as those of normal stress; however they are similar in the sense that the values of the shear stress in the x direction also changed from negative to positive within the potato, which causes a further irregular deformation.

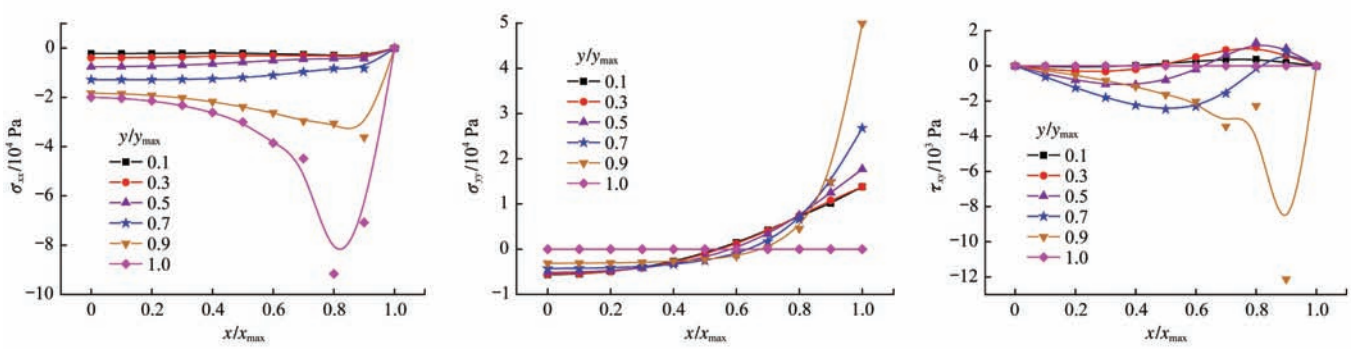

a. Distribution of normal stress σ_{xx} b. Distribution of normal stress σ_{yy} c. Distribution of shear stress τ_{xy}

Figure 12 Spatial variation of stress (normal stress and shear stress) in the potato under the drying conditions of Case 3 at the end of drying

4.3.3 Effect of different drying conditions on drying stresses

The drying conditions not only have an effect on the drying rate but also on the drying stress. Based on the above validation of the model, the effects of the drying conditions on the drying stresses were numerically simulated, and the results are illustrated in Figure 13. It can be seen that normal stresses under different drying conditions both reached their maximum value when the average moisture content fell to near 3.4 kg/kg, and that the shear stresses both reached their maximum value when the average moisture content fell to near 2.8 kg/kg.

Figure 13a illustrates the effect of air velocity (v_a) on the drying stresses. It is worth noticing that high values of v_a induce an increase in the maximum value of stresses—including both normal stress and shear stress—which is due to the enhanced heat and mass transfer between the sample and the hot air with higher values of v_a.

The effect of the relative humidity (RH) on the drying stresses is shown in Figure 13b. Low values of RH induce an increase of the maximum value of both normal stress and shear stress, which is due to the enhanced mass transfer between the sample and hot air at lower RH. This can be understood in terms of the important role of v_a in the drying process. In addition, it can be seen that the sample was subjected to a tensile stress at the beginning of drying process caused by the condensation of water vapor in the hot air on the sample (see Figure 9a).

The effect of air temperature (T_a) during drying on the drying stresses was also considered. Figure 13c shows that the effect of air temperature on drying stress is not the same as that of air velocity and relative humidity. At the beginning of the drying process, different air temperatures have a slightly different effect on the maximum values because of the decreasing moisture content. This can be attributed to thermal equilibrium between the sample surface and the hot air during the constant rate drying stage, and the internal temperature being lower than the wet bulb temperature of the air. After this time, however, drying stresses become more markedly affected by T_a due to the increasing temperature of the sample heated by hot air.

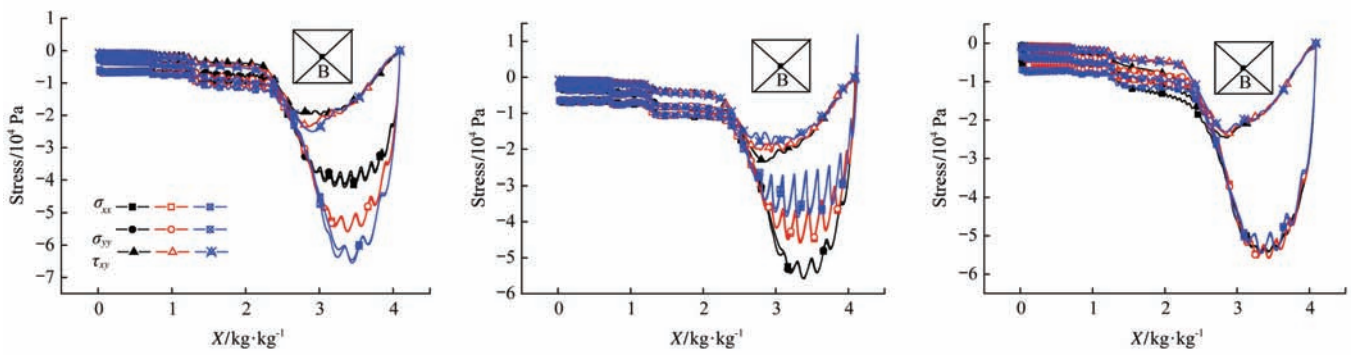

a. T_a=80°C, RH=4.5% b. T_a=80°C, v_a=1 m/s c. v_a=1 m/s, RH=4.5%

Figure 13 Drying stresses under different drying conditions

5 Conclusions

A numerical model was employed to simulate the drying process of deformable porous media using the finite difference method. The feasibility and validity of this model were verified through experiments. The drying curves and the drying stresses were described and their dependence on the drying conditions was discussed. The main conclusions of the present study are as follows:

(1) The drying process of deformable porous media such as potatoes is divided into three stages: the constant speed drying period, the first falling-rate drying period and the second falling-rate drying period. Of these, the constant speed drying period was very short, and sometimes did not appear during drying experiments.

(2) Regarding the effect of drying conditions on the drying process, we can conclude that higher temperature, larger velocity and lower relative humidity of hot air lead to increased drying rate.

(3) Clear deformation behavior of the porous media was observed during drying, and wrinkling was also observed on the surface. The extent of deformation is not affected by the drying conditions, and is completely determined by the moisture content of a particular porous medium.

(4) A detailed analysis of the temporal and spatial distribution of internal drying stresses shows that the sample is subjected to compressive stress in the direction of moisture diffusion. The stress σ_{yy} values changed from negative to positive in the vertical direction, as did the values of shear stress.

(5) Although the extent of deformation is not affected by the drying conditions, drying stresses—in particular, the maximum of the stress—are strongly affected by the drying conditions.

Further extension of this work will consist of performing a study of the drying of anisotropic deformable porous media, as well as a study of their 3D configuration.

Acknowledgements

This work was supported by projects of the Program for New Century Excellent Talents in Universities (No. NCET-13-0651) and Doctoral Scientific Research Foundation of Zhengzhou University of Light Industry. The use of experiment equipment in the laboratory of Prof. Peixue Jiang at Tsinghua University is also acknowledged.

[References]

[1] Baelmans M, Nicolaí B M, Verboven P, Hoang O M L. A continum model for airflow, heat and mass transfer in bulk of chicory roots. Transactions of the ASAE, 2003; 46(6): 1603–1611.

[2] Prado M M, Sartori D J M. Simultaneous heat and mass transfer in packed bed drying of seeds having a mucilage coating. Braz J Chem Eng, 2008; 25(1): 39–50.

[3] Oztop H F, Akpinar E K. Numerical and experimental analysis of moisture transfer for convective drying of some products. Int Commun Heat Mass, 2008; 35(2): 169–177.

[4] Prommas R. Theoretical and experimental study of heat and mass transfer mechanism during convective drying of multi-layered porous packed bed. Int Commun Heat Mass, 2011; 38(7): 900–905.

[5] Toujani M, Hassini L, Azzouz S, Belghith A. Experimental study and mathematical modeling of silverside fish convective drying. J Food Process Pres, 2013; 37(5): 930–938.

[6] Mayor L, Sereno A M. Modelling shrinkage during convective drying of food materials: a review. J Food Eng, 2004; 61(3): 373–386.

[7] Hatamipour M S, Mowla D. Shrinkage of carrots during drying in an inert medium fluidized bed. J Food Eng, 2002; 55(3): 247–252.

[8] Ratti C. Shrinkage during drying of foodstuffs. J Food Eng, 1994; 23(1): 91–105.

[9] Talla A, Puiggali J R, Jomaa W, Jannot Y. Shrinkage and density evolution during drying of tropical fruits: application to banana. J Food Eng, 2004; 64(1): 103–109.

[10] Akpinar E K. Experimental determination of convective heat transfer coefficient of some agricultural products in forced in convection drying. Int Commun Heat Mass, 2004; 31(4): 585–595.

[11] Akpinar E K. Determination of suitable thin layer drying curve model for some vegetables and fruits. J Food Eng, 2006; 73(1): 75–84.

[12] Srikiatden J, Roberts J S. Predicting moisture profiles in potato and carrot during convective hot air drying using isothermally measured effective diffusivity. J Food Eng, 2007; 84(4): 516–525.

[13] Hussain M M, Dincer I. Two-dimensional heat and moisture transfer analysis of a cylindrical moist object subjected to drying: A finite-difference approach. Int J Heat Mass Tran, 2003; 46(21): 4033–4039.

[14] Kadem S, Lachemet A, Younsi R, Kocaefe D. 3d-Transient modeling of heat and mass transfer during heat treatment of wood. Int Commun Heat Mass, 2011; 38(6): 717–722.

[15] Golestani R, Raisi A, Aroujalian A. Mathematical modeling on air drying of apples considering shrinkage and variable diffusion coefficient. Dry Technol, 2013; 31(1): 40–51.

[16] Hu L, Péron H, Hueckel T, Laloui L. Drying shrinkage of deformable porous media: Mechanisms Induced by the Fluid Removal, Computer Applications In Geotechnical Engineering 2007.

[17] Thibeault F, Marceau D, Younsi R, Kocaefe D. Numerical and experimental validation of thermo-hygro-mechanical behaviour of wood during drying process. Int Commun Heat Mass, 2010; 37(7): 756–760.

[18] Islam R, Mujumdar A S. Role of product shrinkage in drying rate predictions using a liquid diffusion model. Int Commun Heat Mass, 2003; 30(3): 391–400.

[19] Yan Z, Sousa-Gallagher M J, Oliveira F A R. Shrinkage and porosity of banana, pineapple and mango slices during air-drying. J Food Eng, 2008; 84(3): 430–440.

[20] Kowalski S J, Rybicki A, Rajewska K. Optimal control of convective drying of saturated porous materials. Aiche J, 2013; 59(12): 4846–4857.

[21] Kowalski S J, Smoczkiewicz-Wojciechowska A. Stresses in dried wood. Modelling and experimental identification. Transp Porous Med, 2007; 66(1-2): 145–158.

[22] Lu T, Wang H L, Jiang P X. A Thermo-hydro-mechanics bidirectional coupling mathematical model for drying of biological porous medium. Dry Technol, 2015; 33(4): 420–428.

[23] Wang H, Lu T, Jiang P. Mathematical model and numerical simulation of biological porous medium during hot air drying. Transactions of the CSAE, 2014; 30(20): 325–333. (in Chinese with English abstract)

[24] Itaya Y, Kobayashi T, Hayakawa K-I. Three-dimensional heat and moisture transfer with viscoelastic strain-stress formation in composite food during drying. Int J Heat Mass Tran, 1995; 38(7): 1173–1185.

[25] Yu C M. Numerical analysis of heat and mass transfer for porous materials (A Theory of Drying). Beijing: Tsinghua University Press, 2011.

[26] Saada A S. Elasticity: theory and applications. APPL MECH REV, 2009; 63(6): 1189–1196.

[27] Bird R B, Stewart W E, Lightfoot E N. Transport Phenomena. second ed, New York: John Wiley & Sons Inc, 2007.

[28] Yang Z R. Principles of Chemical Industry. second ed, Beijing: Chemical Industry Press, 2009.

[29] Chemkhi S, Zagrouba F, Bellagi A. Mathematical model for drying of highly shrinkable media. Dry Technol, 2004; 22(5): 1023–1039.

[30] Hassini L, Azzouz S, Peczalski R, Belghith A. Estimation of potato moisture diffusivity from convective drying kinetics with correction for shrinkage. J Food Eng, 2007; 79(1): 47–56.

[31] Lei D T, Ma X Y. Mechanical properties of potato under broken and its rheology model. Transactions of CSAM, 1991; (2): 63–67. (in Chinese with English abstract)

[32] Mezhericher M, Levy A, Borde I. Modelling of particle breakage during drying. Chemical Engineering and Processing, 2008; 47(8): 1410–1417.

[33] Arrieche L, Corrêa R, Sartori D. Drying stresses and strains in a spherical food model. Computers & Chemical Engineering, 2009; 33(11): 1805–1813.

[34] Zhou Y, Lin G, Gong F X, Liu S L, Zhang D S. Variation between the maximum principal stress and horizontal strain during single fold deformation and its controlling factors. Geotectonica et Metallogenia, 2007; 31(1): 37–43.